

NADPH oxidase-2 derived superoxide drives mitochondrial transfer from bone marrow stromal cells to leukemic blasts

*Christopher R Marlein¹, *Lyubov Zaitseva¹, Rachel E Piddock¹, Stephen Robinson², Dylan Edwards¹, Manar S Shafat¹, Zhigang Zhou¹, Matthew Lawes³, **Kristian M Bowles^{1,3}, **Stuart A Rushworth¹

¹Norwich Medical School, The University of East Anglia, Norwich Research Park, NR4 7TJ, United Kingdom

²School of Biological Sciences, The University of East Anglia, Norwich Research Park, NR4 7TJ, United Kingdom

³Department of Haematology, Norfolk and Norwich University Hospitals NHS Trust, Colney Lane, Norwich, NR4 7UY, United Kingdom

*denotes joint first author

** denotes joint corresponding author

Running title: NOX2 drives mitochondrial transfer to AML

Corresponding Author: email: s.rushworth@uea.ac.uk

Dr Stuart Rushworth

Department of Molecular Haematology,

Norwich Medical School,

University of East Anglia,

Norwich, NR4 7TJ,

United Kingdom: Tel:01603 591802

Word count for text: 2779; abstract: 145, figure 7; reference count: 30

Key points

- Functional mitochondria are transferred in–vivo from BMSC to the leukemic blast.
- AML derived NOX-2 drives transfer of mitochondria via the generation of superoxide.

Abstract

Improvements in the understanding of the metabolic cross-talk between cancer and its micro-environment is expected to lead to novel therapeutic approaches. Acute myeloid leukemia (AML) cells have increased mitochondria compared to non-malignant CD34+ hematopoietic progenitor cells. Furthermore, contrary to the Warburg hypothesis, (AML) relies on oxidative phosphorylation to generate ATP. Here we report that in human AML NOX2 generates superoxide, which stimulates bone marrow stromal cells (BMSC) to AML blast transfer of mitochondria through AML derived tunnelling nanotubes. Moreover, inhibition of NOX2 was able to prevent mitochondrial transfer, dramatically increase AML apoptosis and increase NSG mouse survival. Conversely, mitochondrial transfer could only be stimulated from BMSC to non-malignant CD34+ cells in response to oxidative stress. However, NOX2 inhibition had no detectable effect on non-malignant CD34+ cell survival. Taken together we identify tumor-specific dependence on NOX2 driven mitochondrial transfer as a novel therapeutic strategy in AML.

Acute myeloid leukemia (AML) is an aggressive disease that originates in the bone marrow from malignant transformation of a myeloid progenitor cell. AML can occur at any age but primarily affects the elderly, with the average age at diagnosis of 72 years and three quarters of patients diagnosed after the age of sixty¹. Despite existing cytotoxic treatments directly targeting the leukemic cell two-thirds of younger adults and 90% of older adults will die of their disease². Moreover, current aggressive chemotherapy regimens are often poorly tolerated by the older less fit patients. Improved outcomes are expected to be achieved through novel therapies which are developed from an improved understanding of the biology of the disease.

AML blasts cultured in vitro undergo high levels of apoptosis, however the tumor rapidly proliferates in vivo demonstrating that the tissue microenvironment plays a fundamental role in the development of AML disease^{3,4}. The bone marrow microenvironment consists of many cell types not directly involved in haematopoiesis. These include endothelial cells; osteoclasts; osteoblasts; adipocytes and fibroblasts⁵, which are broadly classed as bone marrow stromal cells (BMSCs) and have previously been shown to support AML survival and contribute to chemotherapy resistance⁶.

In general cancer cells depend on aerobic glycolysis to generate ATP, as hypothesised by Warburg in 1956⁷ and this is thought to be due to activation of oncogenes that promote glycolysis⁸. However the metabolism of AML blasts differs from most other cancers in so much as AML is primarily dependent on mitochondrial oxidative phosphorylation for survival⁹. It is also established that AML cells have higher mitochondria levels compared to non-malignant haematopoietic stem cells^{10,11}, which is entirely consistent with the observations that the tumor is dependent on a mitochondrial ATP production pathway. This proposes a key question; are the additional mitochondria in the AML blasts generated within the tumor cell or have they been acquired?

For a long time mitochondria were thought to be retained in their somatic cell for their lifetime, however in 2004 the Gerdes lab showed that mitochondria can be transferred between cells¹². The main cell type in the bone marrow microenvironment, BMSC have been shown to donate their mitochondria to lung

epithelial cells preventing acute lung injury¹³. This would suggest that BMSC have the capacity to donate their mitochondria within the bone marrow niche. In the present study we look to identify if and how BMSC transfer their mitochondria to AML blasts. Furthermore, we evaluate the mechanisms controlling the increase in mitochondria in AML blasts and finally whether blocking this process is specifically lethal to the tumor but not to the counterpart non-malignant hematopoietic progenitor cells in the bone marrow.

Methods

Materials

Anti-CD45-FITC, anti-CD33-APC, anti-CD90-FITC, anti-CD73-PE, anti-CD105-APC antibodies and CD34 microbeads were purchased from Miltenyi Biotec (Auburn, CA, USA). CellROX green, MitoTracker Green FM and Vybrant Dil stain were purchased from ThermoFisher (Waltham, MA, USA). Human Mitochondrial DNA (mtDNA) Monitoring Primer Set and the rLV.EF1.mCherry-mito-9 Lentivirus were purchased from Clontech Takara Bio Europe (Saint-Germain-en-Laye, France). Murine mitochondrial to nuclear DNA ratio kit was purchased from Detroit R&D (Detroit, MI, USA). All other reagents were obtained from Sigma-Aldrich (St Louis, MO, USA), unless otherwise indicated.

Primary cell culture and differentiation

Primary AML blasts were obtained from patient bone marrow following informed consent and under approval from the UK National Research Ethics Service (LRCERef07/H0310/146). Non-malignant CD34+ haematopoietic stem cells (HSC) were obtained from peripheral blood venesections from normal patients. AML cell isolation was carried out by density gradient centrifugation using Histopaque (Sigma-Aldrich) and cell type was confirmed by flow cytometry as previously described¹⁴. CD34+ HSC were isolated using density gradient centrifugation and CD34+ microbeads (Miltenyi Biotec). Bone marrow stromal cells (BMSC) were isolated by adherence to tissue culture plastic and were then expanded in Dulbecco's Modified Eagle's Medium (DMEM) containing 20% foetal bovine serum (FBS) and supplemented with 1% penicillin-streptomycin (Hyclone, Life Sciences). BMSC markers were confirmed using flow cytometry for expression of CD90+, CD73+, CD105+ and CD45-.

Flow cytometry

For this study we used the CyFlow Cube 6 (Sysmex, Milton Keynes, UK). Cells were incubated for 5 minutes with the FCR receptor blocker (Miltenyi Biotec, Cat. 130-059-901) and then stained with isotype controls or test antibodies (Miltenyi Biotec). Gates were set to the appropriate isotype control.

Mitochondrial Mass determination

To assess mitochondrial DNA copy number we performed direct qRT-PCR of primary cells using Terra qPCR Direct Polymerase mix and Human Mitochondrial DNA (mtDNA) Monitoring Primer Set (Clontech Takara Bio Europe) according to manufactures protocols.

MitoTracker based mitochondrial transfer assay

Human primary BMSC were stained with 200nM MitoTracker Green FM for 1 hour. Primary AML blasts were also stained with 200nM MitoTracker Green FM for 30 mins. Both cell types were washed three times in phosphate buffered saline (PBS) to remove the unbound probe. Stained AML blasts were added to stained BMSC at a 5:1 ratio for 24 hours. Stained AML were also grown in mono-culture for 24 hours as a control. After incubation AML were removed from BMSC and MitoTracker fluorescence in these cells was analysed using the CyFlow Cube 6 flow cytometer (Sysmex, Milton Keynes). This assay was used to quantify mitochondrial transfer to determine the stimulus mechanism, the difference in MitoTracker fluorescence between AML blasts grown with and without BMSC provided a baseline mitochondrial transfer. A pharmacological screen was carried out, whereby numerous drugs and pathway inhibitors were added to the MitoTracker based co-culture, glutathione, hydrogen peroxide and diphenyleneiodonium chloride (Sigma Aldrich) were used further with additional patient AML blasts.

AML xenograft model

All in-vivo studies were carried out following approvals from the UK home office and Animal Welfare and Ethics Board of the University of East Anglia. For this study the NOD.Cg-Prkdcscid IL2rgtm1Wjl/SzJ (NSG) mice (The Jackson Laboratory, Bar Harbour, ME, USA) were housed under specific pathogen-free conditions in a 12/12-hour light/dark cycle with food and water provided *ad libitum* in accordance with the Animal (Scientific Procedures) Act, 1986 (UK). 2×10^6 primary AML blasts were intravenously injected into non-irradiated 6-8 week old NSG mice. 2.5×10^5 OCI-AML3-luc cells were injected, as per the primary blasts, for the NOX-2 KD xenograft. Mice injected with OCI-AML3-luc cells were monitored via in vivo bioluminescent imaging (Bruker, Coventry UK). At pre-defined humane end points mice were sacrificed (6-12 weeks post injection), bone marrow isolated and engraftment

determined using human CD33 and CD45 expression. Human AML blasts were purified from the heterogeneous bone marrow by MACS using CD45 microbeads. This purified human AML blast population was used for the PCR and agarose gel electrophoresis. Levels of mitochondria in the purified OCI-AML3-luc populations was achieved using MitoTracker Green FM staining and flow cytometry.

Murine mitochondrial DNA detection

Murine mitochondrial DNA detection was used to determine if inter-species mitochondrial transfer occurred from murine BMSC to human AML blasts. This method was used for both the *in vitro* culture and *in vivo* study. DNA from the purified human AML blasts was extracted using the GenElute mammalian DNA miniprep kit. 8ng of DNA was added to the PCR reaction containing Sybr green and murine primers provided in the Detroit R&D kit. PCRs were amplified for 40 cycles (95°C/15 seconds, 60°C/60 seconds) on a Roche 96-well LightCycler480. PCR products were run on a 1.25% agarose gel at 100V for 1 hour. Detection was performed by Chemdoc-It2 Imager (UVP) and analysed using ImageJ.

Fluorescence and Confocal Microscopy

Primary human BMSC were transduced with a rLV.EF1. mCherry-Mito-9 Lentivirus and were cultured with primary AML blasts for between 72 hours and 3 weeks. Live cell imaging was carried out in FluoroBrite DMEM media supplemented with 10% FBS (Hyclone, Life Sciences). Cytochalasin B (Sigma Aldrich) was added to the culture to analyse tunnelling nanotube formation (TNT). To visualise TNTs BMSC were stained with 100nM MitoTracker green FM and AML were stained with Vybrant Dil stain to visualise cell membranes. After co-culture cells were fixed with 4% paraformaldehyde and imaged. Fluorescence and bright field images were acquired on Zeiss Axio Vert.A1 microscope with 20X and 40X air objectives (Carl Zeiss) confocal images were acquired on Zeiss LSM 800 Axio Observer.Z1 confocal microscope with 40X and 63X water objectives (Carl Zeiss).

2',7'-dichlorodihydrofluorescein diacetate (H₂DCFDA) and CellROX assays

BMSC after a 24h co-culture with primary AML blasts were stained with 20µM H₂DCFDA (Sigma Aldrich) for 30 mins at 37°C in FluoroBrite DMEM media supplemented with 10% FBS, BMSC grown alone were also stained. After incubation

cell were washed in PBS before flow cytometry analysis of the H2DCFDA fluorescence. Live fluorescence microscopy cell imaging was also used to visualise BMSC ROS. AML cells were not removed from the BMSC, H₂O₂ and NAC were also used with the same concentrations as the MitoTracker pre-stain assay.

For the CellROX assay BMSC were cultured with primary AML blasts for 24 hours or stimulated with H₂O₂ and then stained with 10µM CellROX green reagent (ThermoFisher Waltham, MA, USA) for 30 minutes. After incubation the cells were washed with PBS and analysed using confocal microscopy.

Lentiviral transduction

NOX-2 shRNA glycerol stock was purchased from Sigma Aldrich (TRCN0000064588). Lentivirus particles generated using this construct were produced as previously described¹⁵. Lentiviral stocks were concentrated using Amicon® Ultra centrifugal filters and titres were determined using Lenti-X™ qRT-PCR titration kit (CloneTech). Primary AML blasts were plated at a density of 5x10⁴/well in a 24 well plate and infected with the NOX-2 lentivirus at MOI 30. NOX-2 knockdown was confirmed using qRT-PCR.

Real-time polymerase chain reaction

Reverse transcription was performed using an RNA polymerase chain reaction (PCR) core-kit (Applied Biosystems). Relative quantitative real-time (qRT)-PCR used SYB-green technology (Roche) on generated complementary DNA. After pre-amplification (95°C/60 seconds), PCRs were amplified for 45 cycles (95°C/15 seconds, 60°C/10 seconds, 72°C/10 seconds) on a Roche 384-well LightCycler480. Messenger RNA (mRNA) expression was normalized against glyceraldehyde 3-phosphate dehydrogenase (GAPDH).

Apoptosis

Apoptosis of AML blasts and non-malignant CD34+ HSC was measured using PI/AnnexinV (eBiosciences) after co-culture with AML blasts and was quantified using flow cytometry.

Amplex Red Superoxide Assay

The amplex red hydrogen peroxide/peroxidase assay kit was used to determine superoxide production was control KD vs NOX-2 KD AML blasts. 1×10^5 cells were plated in a 96 well plate for 48 hours in FluoroBrite DMEM media supplemented with 10% FBS. The assay was carried out as per manufacturer's protocol with a H_2O_2 standard curve allowing superoxide quantification.

Mitochondrial Respiration

Mitochondrial respiration in AML blasts was assessed using the Seahorse XFp Analyzer, as previously described ¹⁶, and the Seahorse XF Mito stress test kit (Agilent Seahorse Bioscience) according to manufacturer's specifications. Briefly, AML blasts were cultured with or without BMSC and then removed from co-culture and plated in poly-D-lysine (Sigma) coated assay wells at a density of 2×10^5 per well in base media containing 2.5mM glucose, 0.5mM carnitine and 5mM HEPES. Oligomycin ($2 \mu M$), FCCP ($0.25 \mu M$) and Rotenone ($0.5 \mu M$) were added into the injection ports. The experimental template was designed using Wave software for desktop from Seahorse Bioscience. ATP production was monitored by the CellTiter-Glo assay (Promega).

Statistical analysis

We used the Mann-Whitney U test, Wilcoxon matched pairs test and paired t test to compare results between groups. The Mantel-Cox test was used to analyse Kaplan-Meier survival curves. Results with $P < 0.05$ (denoted by *), $P < 0.01$ (denoted by **) $P < 0.001$ (denoted by ***) were considered statistically significant. Results represent the mean \pm Standard Deviation of 4 independent experiments. We generated statistics with Graphpad Prism 5 software (Graphpad, San Diego, CA, USA).

Results

BMSC donate their mitochondria to leukemic blasts.

As previously reported human AML blasts have an increased mitochondrial mass compared to non-malignant CD34+ progenitor cells^{10,11} (Figure 1A). To determine if BMSC support the increase of mitochondria in AML we examined mitochondrial content after in-vitro co-culture. Figure 1B shows that AML increase their mitochondrial mass after co-culture with BMSC. Next we used 3 different methods to show that BMSC transfer their mitochondria to primary human AML.

First, we assessed mitochondrial transfer between our patient derived BMSC and primary AML blasts by infecting BMSC with a rLV.EF1.mCherry-Mito-9 Lentivirus for stable production of mitochondria incorporated mCherry tagged protein. Using this we observed that primary AML blasts, after co-culture with these BMSC, acquired the mCherry fluorescence (Figure 1C and 1D). This demonstrates that mitochondria from the BMSC with the mCherry tag move to the AML blasts.

Second, we used MitoTracker Green FM stain to quantify mitochondria in AML after co-culture with BMSC. We incubated both BMSC and AML with MitoTracker Green FM stain for 1h. The cells were washed twice in PBS and incubated for 4 h. The cells were then co-cultured for 24 h and then measured for MitoTracker fluorescence using flow cytometry. Figure 1E shows that AML in cultured with BMSC had significantly more mitochondria than AML cells cultured alone. This was also the case for the OCI-AML3 cell line (Supplementary Figure 1A). To begin to address whether this is a tumor specific phenomenon we repeated the experiment using non-malignant CD34+ cells in the BMSC assay and showed no significant increase in MitoTracker fluorescence in the hematopoietic progenitor cells (Figure 1F).

Third, we used an in-vivo xenograft model in which human primary AML were transplanted into NSG mice. Following tumor engraftment we determined if mouse mitochondrial DNA (mtDNA) could be detected in the human leukemia cells after extraction from NSG bone marrow. Four individual patient AML samples were transplanted into 8 NSG mice and following engraftment at between 6 and 12 weeks human AML blasts were isolated via human CD45 sorting (Figure 2A). Primary AML blasts reliably engrafted into NSG mice, verified by human CD33 and CD45

expression confirming human AML blast identity (Figure 2B) and Figure 2C shows that the human CD45 sorted cells were a pure population. Next we wanted to determine if the engrafted AML and subsequent CD45 purified human blasts had acquired mouse mitochondria. To do this we performed a PCR analysing mouse mitochondrial DNA and mouse genomic DNA. Figure 2D shows that AML blasts isolated from engrafted NSG mice contained mouse mitochondrial DNA but not mouse genomic DNA, this was also the case for the OCI-AML3 cell line (Figure 2E). Taken together these 3 methods show that mitochondria are transferred from BMSC to leukemic blasts both in vitro and in vivo.

Mitochondria transfer occurs via leukemia derived tunnelling nanotubule (TNT)

A constant observation from live cell imaging was that AML blasts that acquire the mCherry fluorescence are in direct contact with the BMSC, this led us to investigate whether a cell-cell interaction is the way mitochondria move between the two cell types (figure 1C). We first hypothesised that tunnelling nanotubes (TNT) facilitate mitochondrial transfer from BMSC to AML blasts. To inhibit TNT formation we added cytochalasin B to our mCherry-Mito-9 BMSC-AML co-culture experiment. Figure 3A and 3B show that there is a significant reduction in the percentage of AML blasts that acquire the mCherry fluorescence after cytochalasin B treatment. This suggests that mitochondria from the BMSC are transferred to the AML blast via TNTs.

TNTs are functionally dynamic, so in order to visualise the transfer of mitochondria we used a fixed cell based imaging. To do this we stained AML blasts with the Vybrant lipid stain (red) and the mitochondria in BMSC cells with MitoTracker Green FM stain and then cultured the cells together for 24 hours. Following co-culture the cells were fixed and TNT formation was detected using confocal microscopy. In Figure 3C we observed green mitochondria from the BMSC in the red TNT projecting from the AML blasts.

ROS regulates the transfer of mitochondria from BMSC to leukemia blasts

It is not known what stimulates mitochondrial transfer in AML or any cancer. Moreover, determination of the controlling stimulus is essential if this biological phenomenon is to be exploited therapeutically in the future.

To identify the mechanism of mitochondrial transfer in AML we used a pharmacological screen in which the MitoTracker experiment described in Figure 1 was employed as a screening tool. Figure 4A shows that N-acetyl cysteine (NAC), glutathione (GSH) and diphenyleneiodonium (DPI) inhibit mitochondrial transfer. In contrast we observe that hydrogen peroxide (H_2O_2), daunorubicin and cobalt chloride further enhance mitochondrial transfer from BMSC to AML blasts. In our baseline experimental conditions mitochondria did not transfer from BMSC to non-malignant CD34+ cells (Figure 1F). However, the addition of H_2O_2 to the co-culture of non-malignant CD34+ cells and BMSC co-cultures was able to induce mitochondrial transfer to the CD34+ cells. Next we wanted to determine if AML blasts are responsible for an increase in ROS levels in BMSC. To do this we analysed BMSC ROS when cultured with AML using two assays CellROX and 2',7'-dichlorodihydrofluorescein diacetate (H2DCFDA) assay. Figure 4E, F and G shows that culture with AML blasts causes increased ROS levels and oxidative stress in the BMSC. Figure 4H shows that non-malignant CD34+ cells do not increase ROS levels in BMSC. Taken together these results, show that AML induced ROS stimulate mitochondrial transfer from BMSC.

AML derived NOX-2 drives mitochondrial transfer

We observed that diphenyleneiodonium (DPI) was able to inhibit mitochondrial transfer in our assays (Figure 5A, Supplementary Figure 1B). As DPI inhibits NOX-2, and NOX-2-derived ROS plays a critical role in mobilization and homing of non-malignant hematopoietic stem cells ¹⁷, we next asked whether NOX-2 derived superoxide produced by the AML was responsible for mitochondrial transfer. We knocked down NOX-2 using a lentiviral transduction (Figure 5B) in 4 human AML patient cell samples and the OCI-AML3 cell line. Then we analysed mitochondrial transfer to AML following NOX-2 or control shRNA knockdown. Figure 5C shows a significant reduction in mitochondrial transfer in the NOX-2 KD AML cells compared to control KD blasts, also consistent with the OCI-AML3 cell line (Supplementary Figure 1C). To confirm that superoxide was reduced in the NOX-2 KD cells we analysed superoxide using the AmplexRED assay. Figure 5D shows that NOX-2 KD cells have significantly reduced superoxide. Next we tested if AML with NOX-2 KD could increase ROS in BMSC. Figure 5E shows that NOX-2 KD AML cells had a reduced capacity to stimulate ROS production in the BMSC compared to control KD

blasts. Finally, we tested if DPI could reduce survival of AML in culture with BMSC. Figure 5F shows that AML blast survival on BMSC is inhibited by the addition of DPI. Moreover, DPI had little or no effect on the viability of non-malignant CD34+ cells grown in co-culture with BMSC (Figure 5G). Taken together in leukemic blasts NOX2 derived superoxide stimulates ROS generation in BMSC which results in mitochondrial transfer from the stroma to the tumor.

Mitochondria acquired by the AML blast are functionally active and contribute to the metabolic capacity

We next explored the function of mitochondrial transfer in relation to mitochondrial respiration. We found that after co-culture with BMSC AML blasts have increased basal and maximum mitochondrial respiration compared control cells (Figures 6A and 6B). In addition, the ATP production capacity of AML blasts in co-culture with BMSC was increased compared to control cells (Figure 6C). This shows that mitochondria in AML after co-culture with BMSC are functional and contribute to energy requirements of the rapidly proliferating cancer cell. To determine if the mitochondria transferred are responsible for this increased respiration, we analysed the mitochondrial respiration in the control and NOX-2 knockdown primary AML blasts in co-culture with BMSC. We found that knockdown blasts had significantly reduced basal and maximum mitochondrial respiration (Figure 6D), showing that mitochondrial transfer has to occur in order for AML to have increased mitochondrial output when cultured with BMSC.

NOX-2 is crucial for the development of AML in an *in vivo* xenograft model

To analyse in the impact of NOX-2 on mitochondrial transfer and disease progression, we engrafted control KD and NOX-2 KD OCI-AML3-luc cells into NSG mice. Mice were imaged using bioluminescence at weekly intervals. These images revealed that there is reduced AML disease progression and engraftment in the bone marrow with NOX-2 KD cells compared to the control KD cells (Figure 7A). Disease progression was monitored until humane end point, the survival of the NOX-2 KD mice was significantly increased compared to the control KD mice (Figure 7B). OCI-AML3-luc reliably engrafted into NSG mice, verified by human CD45 expression confirming human AML blast identity (Figure 7C). Mitochondrial levels were analysed in the two cell populations pre and post engraftment into the NSG mice, using

MitoTracker Green FM. There was no difference in the mitochondrial levels between the control and NOX-2 KD pre-engraftment (Figure 7D). However in the purified OCI-AML3-luc cells post engraftment, the control KD cells had significantly increased mitochondrial levels compared to NOX-2 KD cells (Figure 7E). Taken together these results show that there is reduced mitochondrial transfer in vivo to NOX-2 KD cells compared to control KD cells. This reduces the engraftment and disease progression in these cells and enhances survival.

Discussion

In this study we report that BMSC within the protective microenvironment of AML transfer their mitochondria to AML blasts. Furthermore, we show that mitochondria are transferred via AML-derived TNTs. We identified that AML derived ROS drives mitochondrial transfer from the BMSC to the AML. Specifically, NOX-2 derived superoxide generated from the AML causes mitochondrial transfer, shown through in vitro and in vivo studies. We were able to reduce mitochondrial transfer using both lentiviral knockdown and pharmacological inhibition of NOX2. Overall our results provide a first in cancer mitochondrial transfer mechanism, whereby the cancer cell drives transfer through increasing oxidative stress in the non-malignant donor cell.

Mitochondrial transfer is known to occur in other cancers such as breast¹⁸, lung¹⁹ and melanoma²⁰. Our work shows in patient derived AML blast and BMSC samples, using three in vitro methods and an in vivo model that mitochondrial transfer was also observed between the BMSC and the AML blast. The mitochondria that move to the AML are also functionally active, highlighting that the AML blast is using this biological phenomenon to its metabolic advantage. As Mitochondrial transfer has been shown to occur via TNTs in some cancers^{18,21,22}, whereas in other disease contexts it has been shown to be via connexin-43 GAP junctions¹³. A constant observation was that AML blasts which acquired mitochondria were in contact with BMSC, therefore we first analysed whether the mitochondria could be moving via TNTs in our AML cancer setting. Through the addition of cytochalasin B to the co-culture and capturing the dynamic interactions through confocal microscopy, we report that mitochondria move from BMSC to AML blasts predominantly through TNTs. In previous literature presenting mitochondrial transfer in AML it was suggested that mitochondria moved between cells via endocytosis²³. Our results do not disprove this idea and it is possible a combination of the two mechanisms (or possibly more) contribute to the total mitochondria that are acquired by the AML blast. The TNT mechanism is however necessary for AML survival.

Through the pharmacological screen we highlighted that inducing ROS increased mitochondrial transfer, whereas inhibiting ROS reduced transfer. Additionally, we found that AML blasts increase oxidative stress in the BMSC. Chronic oxidative stress has been shown to aid tumour survival²⁴, metastasis²⁵ and proliferation²⁶. It

is also known that there are high levels of oxidative stress in AML ²⁷ and that in AML disease relapse there are increased markers of oxidative stress ²⁸. As we have shown oxidative stress drives mitochondrial transfer, this biological phenomenon may be the underlying reason why oxidative stress promotes AML proliferation and relapse. Interestingly using H₂O₂ we could stimulate mitochondrial transfer to non-malignant CD34+ cells, which do not otherwise acquire mitochondria under baseline conditions, AML acts in a *'parasitic'* way by generating the hypoxic conditions in the bone marrow necessary for mitochondrial transfer from stromal cells.

We show that specifically NOX-2 generated superoxide derived from the AML blasts drives the observed mitochondrial transfer, which provides a molecular target for the process. NOX-2 has an established role in immune defence whereby superoxide produced by NOX-2 on phagocytic myeloid cells destroys pathogens ²⁹. Through DPI drug inhibition of NOX-2 we show that in co-culture with BMSC, the cell viability of AML blasts is significantly reduced highlighting the significance of NOX-2 in AML disease. NOX-2 knockdown blasts have reduced mitochondrial respiration compared to control knockdown cells, therefore the metabolic requirements of the blasts may not be met resulting in the observed cell death. Inhibition of NOX-2 in vivo highlighted that NOX-2 and the resultant mitochondrial transfer is essential for AML disease progression, whereby NSG mice administered with NOX-2 KD AML out survived their control counterparts. Interestingly in vitro, the cell viability of non-malignant CD34+ cells is unaffected upon the addition of DPI to the co-culture. It has been previously described that AML blasts produce a greater quantity of NOX-2 derived superoxide than non-malignant CD34+ cells ³⁰. This knowledge combined with the fact non-malignant CD34+ cells do not acquire mitochondria from BMSC and do not stimulate oxidative stress in the BMSC opens up a novel therapeutic window. Mitochondrial transfer from BMSC could be targeted therapeutically through NOX-2 inhibition without any detrimental effects to the normal haematopoietic system.

Overall we report a first in cancer mitochondrial transfer mechanism whereby NOX-2 derived oxidative stress drives transfer from non-malignant BMSC to AML blasts. Moreover, we show that this mitochondrial transfer is fundamentally a part of the malignant AML phenotype. Accordingly, these results may have the ability to be

translated into other malignancies where mitochondrial transfer has previously been observed but, where the specific mechanism have yet to be elucidated. Finally, our results identify a novel therapeutic opportunity to be developed and explored for the treatment of AML.

Acknowledgments

The authors wish to thank the Rosetrees Trust, The Big C and the Norwich Research Park Doctoral Training Program for funding. Additionally, thanks to Professor Richard Ball, Dr Mark Wilkinson and Mr Iain Sheriffs, Norwich Biorepository (UK) for help with sample collection and storage. pCDH-luciferase-T2A-mCherry was kindly gifted from Prof. Dr. med. Irmela Jeremias, Helmholtz Zentrum München, Munchen, Germany.

Author contributions

Authorship contributions

C.R.M., L.Z., K.M.B and S.A.R designed the research; C.R.M., L.Z., R.E.P and M.S.S., performed the research; S.A.R., C.R.M., S.D.R., and R.E.P. carried out in vivo work; D.R.E., Z.Z., M.L. and K.M.B. provided essential reagents and knowledge. C.R.M., L.Z., K.M.B., and S.A.R. wrote the paper.

Conflict of interest

All authors declare no competing financial interests.

References

1. Juliusson G, Antunovic P, Derolf A, et al. Age and acute myeloid leukemia: real world data on decision to treat and outcomes from the Swedish Acute Leukemia Registry. *Blood*. 2009;113(18):4179-4187.
2. Rowe JM, Tallman MS. How I treat acute myeloid leukemia. *Blood*. 2010;116(17):3147-3156.
3. Matsunaga T, Takemoto N, Sato T, et al. Interaction between leukemic-cell VLA-4 and stromal fibronectin is a decisive factor for minimal residual disease of acute myelogenous leukemia. *Nat Med*. 2003;9(9):1158-1165.
4. Rushworth SA, Pillinger G, Abdul-Aziz A, et al. Activity of Bruton's tyrosine-kinase inhibitor ibrutinib in patients with CD117-positive acute myeloid leukaemia: a mechanistic study using patient-derived blast cells. *Lancet Haematol*. 2015;2(5):e204-211.
5. Zimmerlin L, Donnenberg VS, Rubin JP, Donnenberg AD. Mesenchymal markers on human adipose stem/progenitor cells. *Cytometry A*. 2013;83(1):134-140.
6. Abdul-Aziz AM, Shafat MS, Mehta TK, et al. MIF-Induced Stromal PKC β /IL8 Is Essential in Human Acute Myeloid Leukemia. *Cancer Res*. 2017;77(2):303-311.
7. Warburg O. On the origin of cancer cells. *Science*. 1956;123(3191):309-314.
8. Duvel K, Yecies JL, Menon S, et al. Activation of a metabolic gene regulatory network downstream of mTOR complex 1. *Mol Cell*. 2010;39(2):171-183.
9. Suganuma K, Miwa H, Imai N, et al. Energy metabolism of leukemia cells: glycolysis versus oxidative phosphorylation. *Leuk Lymphoma*. 2010;51(11):2112-2119.
10. Boulwood J, Fidler C, Mills KI, et al. Amplification of mitochondrial DNA in acute myeloid leukaemia. *Br J Haematol*. 1996;95(2):426-431.
11. Skrtic M, Sriskanthadevan S, Jhas B, et al. Inhibition of mitochondrial translation as a therapeutic strategy for human acute myeloid leukemia. *Cancer Cell*. 2011;20(5):674-688.
12. Rustom A, Saffrich R, Markovic I, Walther P, Gerdes HH. Nanotubular highways for intercellular organelle transport. *Science*. 2004;303(5660):1007-1010.
13. Islam MN, Das SR, Emin MT, et al. Mitochondrial transfer from bone-marrow-derived stromal cells to pulmonary alveoli protects against acute lung injury. *Nat Med*. 2012;18(5):759-765.

14. Zaitseva L, Murray MY, Shafat MS, et al. Ibrutinib inhibits SDF1/CXCR4 mediated migration in AML. *Oncotarget*. 2014;5(20):9930-9938.
15. Rushworth SA, Zaitseva L, Murray MY, Shah NM, Bowles KM, MacEwan DJ. The high Nrf2 expression in human acute myeloid leukemia is driven by NF- κ B and underlies its chemo-resistance. *Blood*. 2012;120(26):5188-5198.
16. Shafat MS, Oellerich T, Mohr S, et al. Leukemic blasts program bone marrow adipocytes to generate a pro-tumoral microenvironment. *Blood*. 2017.
17. Urao N, Inomata H, Razvi M, et al. Role of Nox2-Based NADPH Oxidase in Bone Marrow and Progenitor Cell Function Involved in Neovascularization Induced by Hindlimb Ischemia. *Circulation research*. 2008;103(2):212-220.
18. Pasquier J, Guerrouahen BS, Al Thawadi H, et al. Preferential transfer of mitochondria from endothelial to cancer cells through tunneling nanotubes modulates chemoresistance. *J Transl Med*. 2013;11:94.
19. Spees JL, Olson SD, Whitney MJ, Prockop DJ. Mitochondrial transfer between cells can rescue aerobic respiration. *Proc Natl Acad Sci U S A*. 2006;103(5):1283-1288.
20. Tan AS, Baty JW, Dong LF, et al. Mitochondrial genome acquisition restores respiratory function and tumorigenic potential of cancer cells without mitochondrial DNA. *Cell Metab*. 2015;21(1):81-94.
21. Lou E, Fujisawa S, Morozov A, et al. Tunneling nanotubes provide a unique conduit for intercellular transfer of cellular contents in human malignant pleural mesothelioma. *PLoS One*. 2012;7(3):e33093.
22. Wang X, Gerdes HH. Transfer of mitochondria via tunneling nanotubes rescues apoptotic PC12 cells. *Cell Death Differ*. 2015;22(7):1181-1191.
23. Moschoi R, Imbert V, Nebout M, et al. Protective mitochondrial transfer from bone marrow stromal cells to acute myeloid leukemic cells during chemotherapy. *Blood*. 2016;128(2):253-264.
24. Clerkin JS, Naughton R, Quiney C, Cotter TG. Mechanisms of ROS modulated cell survival during carcinogenesis. *Cancer Lett*. 2008;266(1):30-36.
25. Wu WS, Wu JR, Hu CT. Signal cross talks for sustained MAPK activation and cell migration: the potential role of reactive oxygen species. *Cancer Metastasis Rev*. 2008;27(2):303-314.

26. Arnold RS, He J, Remo A, et al. Nox1 expression determines cellular reactive oxygen and modulates c-fos-induced growth factor, interleukin-8, and Cav-1. *Am J Pathol.* 2007;171(6):2021-2032.
27. Sallmyr A, Fan J, Rassool FV. Genomic instability in myeloid malignancies: increased reactive oxygen species (ROS), DNA double strand breaks (DSBs) and error-prone repair. *Cancer Lett.* 2008;270(1):1-9.
28. Zhou FL, Zhang WG, Wei YC, et al. Involvement of oxidative stress in the relapse of acute myeloid leukemia. *J Biol Chem.* 2010;285(20):15010-15015.
29. Segal AW, Jones OT, Webster D, Allison AC. Absence of a newly described cytochrome b from neutrophils of patients with chronic granulomatous disease. *Lancet.* 1978;2(8087):446-449.
30. Hole PS, Zabkiewicz J, Munje C, et al. Overproduction of NOX-derived ROS in AML promotes proliferation and is associated with defective oxidative stress signaling. *Blood.* 2013;122(19):3322-3330.

Figure Legends

Figure 1. BMSC donate their mitochondria to leukemic blasts. (A) Mitochondrial DNA copy number was assessed in primary non-malignant CD34+ cells (n=7) and AML blasts (n=9) (P=0.0164). (B) Mitochondrial DNA copy number was assessed in primary AML blasts (n=6) in mono-culture vs co-culture with BMSC for 72 hours and 1 week (P=0.0022). (C) BMSC were transduced with a rLV.EF1. mCherry-Mito-9 Lentivirus. AML blasts were cultured on mCherry-Mito-9 positive BMSC and were analysed by live cell imaging after a 1 week culture. Bright field, mCherry and merged channels are shown. (D) Live cell imaging was repeated with 5 primary AML patient samples, the percentage of mCherry positive AML blasts is presented. (E and F) Primary AML blasts (n=11) or non-malignant CD34+ cells (n=7) were pre-stained with 200nM MitoTracker Green FM for 24 hours on BMSC stained with MitoTracker Green FM, MitoTracker fluorescence was analysed in the AML blasts (P=0.001) and non-malignant CD34+ cells ($p < 0.05$) by flow cytometry.

Figure 2. Human AML acquire mouse mitochondria in NSG xenograft model. (A) schematic representation of PDX model used for these experiments. (B) 2×10^6 primary AML cells (4 individual patient AML) were I.V. injected into NSG mice. Engraftment was measured using human CD33 and human CD45. In the dot plot each AML engraftment into NSG mice is shown for bone marrow and spleen. (C) Engrafted AML were purified from the mouse BM using human CD45 cell sorting. Shown in the flow figure are the characteristics of AML#12 engraftment into BM and spleen. (D) Total DNA was extracted from the purified AML and analysed by PCR for murine and human specific mitochondrial and genomic DNA. PCR products were visualised by agarose gel electrophoresis. (E) OCI-AML3 cells engrafted into NSG mice were also analysed by PCR and agarose gel electrophoresis.

Figure 3. Mitochondria transfer to leukemic blasts occurs via TNT. (A) BMSC were transduced with a rLV.EF1. mCherry-Mito-9 Lentivirus. AML blasts were cultured on mCherry-Mito-9 positive BMSC and were analysed by live cell imaging. With and without cytochalasin B. (B) Multiple primary AML blasts were cultured on rLV.EF1. mCherry-Mito-9 Lentivirus transduced BMSC with and without cytochalasin B the percentage of mCherry positive AML is shown. (C) AML blasts were stained with Vybrant Dil for 1 h and washed 3 times in PBS. BMSC were stained with

MitoTracker green FM for 1 h and washed 3 times in PBS. AML blasts and BMSC were then cocultured for 24 hours before fixation using paraformaldehyde. Cells were visualised by confocal microscopy.

Figure 4. ROS regulate the transfer of mitochondria from BMSC to AML blast.

(A) Primary AML and BMSC were pre-stained with MitoTracker green FM for 1h and then cultured together before 24 h drug treatment. Flow cytometry was used to detect MitoTracker green FM in the AML blast. (B) Primary AML (n=7) and BMSC were pre-stained with MitoTracker green FM for 1h and then cultured together before 24 h NAC (5mM) and GSH (5Mm) treatment. Flow cytometry was used to detect MitoTracker green FM in the AML blast. (C) Primary AML (n=10) and BMSC were pre-stained with MitoTracker green FM for 1h and then cultured together before 24 h H₂O₂ (50µM). Flow cytometry was used to detect MitoTracker green FM in the AML blast. (D) non-malignant CD34+ cells (n=7) and BMSC were pre-stained with MitoTracker green FM for 1h and then cultured together before 24 h H₂O₂ (50µM). Flow cytometry was used to detect MitoTracker green FM in the malignant CD34+ cells. (E) BMSC cultured alone and in co-culture with AML or treated with H₂O₂ (50µM) AML were removed and BMSC were stained for ROS using CellROX. BMSC were visualised for ROS using fluorescence microscopy. (F) BMSC cultured alone and in co-culture with AML or treated with H₂O₂ (50µM) AML were removed and BMSC were stained for ROS using H₂DCFDA (10µM). BMSC were visualised for ROS using fluorescence microscopy or flow cytometry (G) BMSC cultured alone and in co-culture with non-malignant CD34+ cells or treated with H₂O₂ (50µM) AML were removed and BMSC were stained for ROS using H₂DCFDA (10µM). BMSC were visualised for ROS flow cytometry.

Figure 5. AML derived NOX-2 drives mitochondrial transfer.

(A) Primary AML (n=11) and BMSC were pre-stained with MitoTracker green FM for 1h and then cultured together before 24 h treatment with DPI (1µM). (B) 4 AML patient samples were transduced with a lentivirus targeted to NOX-2 or control for 72 h. NOX-2 mRNA levels were analysed by real-time PCR and normalised to GAPDH. (C, D, E and F) 4 AML patient samples were transduced with a lentivirus targeted to NOX-2 or control for 72 h. KD AML cells and BMSC were pre-stained with MitoTracker green FM for 1h and then cultured together before 24 h. MitoTracker was detected

by was detected by flow cytometry. (D) Superoxide production was detected in NOX-2 and control KD AML cells by AmplexRED assay. (E) BMSC were cultured with control KD AML or NOX-2 KD AML. BMSC were stained for ROS using H2DCFDA (10 μ M) and visualised for ROS using flow cytometry. (F) Primary AML or (G) non-malignant CD34+ were cultured with BMSC and treated with DPI (1 μ M) for 72 h. AML blasts or non-malignant CD34+ cells were stained with Annexin V and analysed by flow cytometry.

Figure 6. Mitochondria acquired by the AML blast are functionally active and contribute to the metabolic capacity. (A) Primary AML blasts were grown with and without BMSC for 72 hours and then analysed independently using the Seahorse XFp Analyser with the Mito Stress Test Kit. Data represented as mean \pm standard deviation. Sequential injections of Oligomycin (O), FCCP (F) and Rotenone (R) were used to obtain respiration dynamics presented in (B). (C) Primary AML blasts were grown with and without BMSC and after 72 hours the ATP production capacity was analysed by CellTitre-Glo, with cells numbers normalised. (D) BMSC were cultured with control KD AML or NOX-2 KD AML for 72 hours. The blasts were then analysed using the Seahorse Extracellular Flux Analyser, basal and maximum mitochondrial respiration is presented.

Figure 7. NOX-2 is crucial for the development of AML in an *in vivo* xenograft model. (A) Mice were imaged using bioluminescence weekly to monitor engraftment and disease progression in the animals administered with control and NOX-2 KD cells. (B) The survival of NSG mice administered with either control KD or NOX-2 KD OCI-AML3-luc cells. (C) Engraftment of AML in bone marrow harvested post human end point was analysed by flow cytometry for human CD45 expression. (D) Mitochondrial levels were analysed in the OCI-AML3-luc pre engraftment by staining for 15 mins in 200mM MitoTracker Green FM. (E) Mitochondrial levels in the purified OCI-AML3-luc population were also analysed as in D.

Figure 1

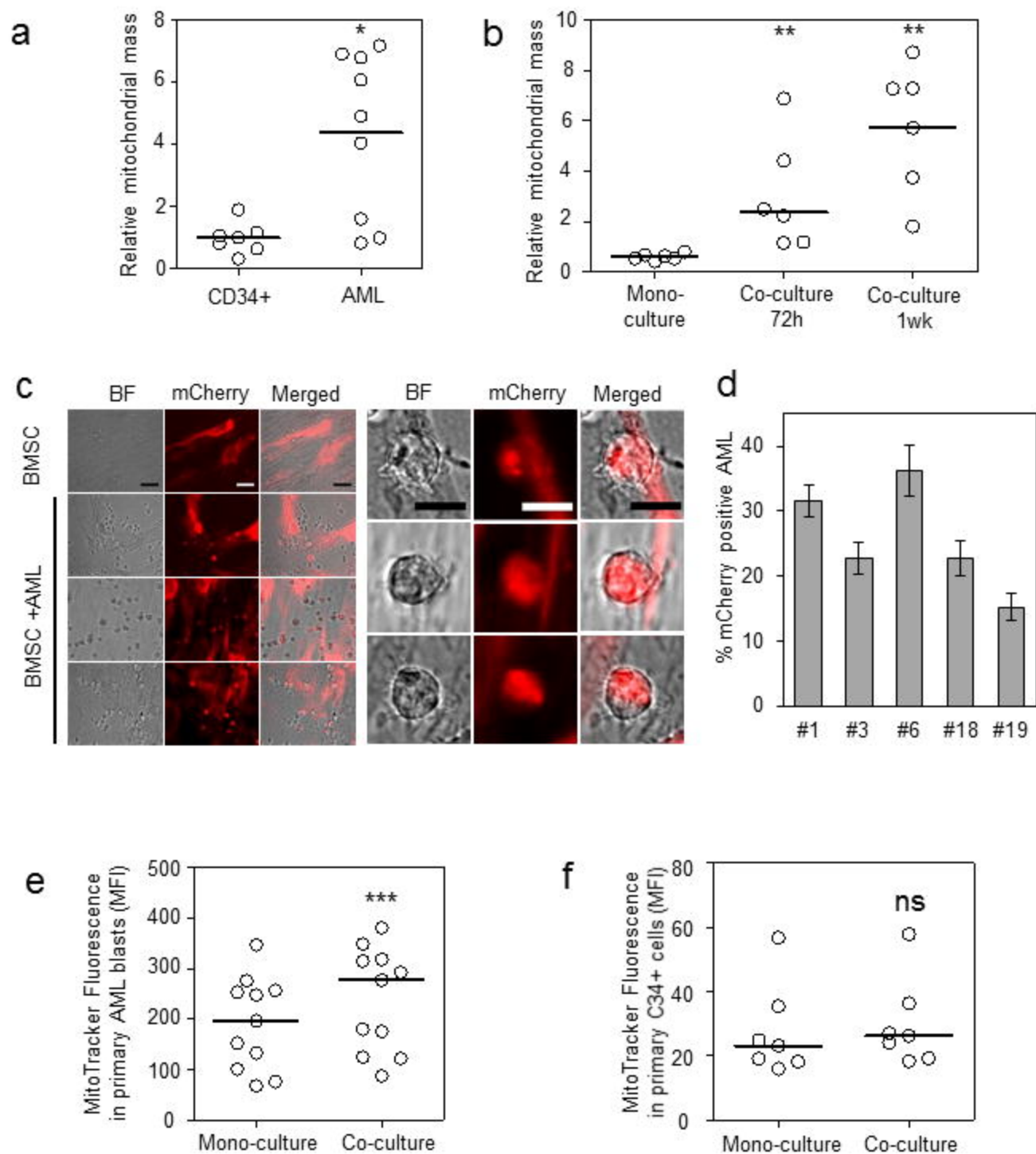
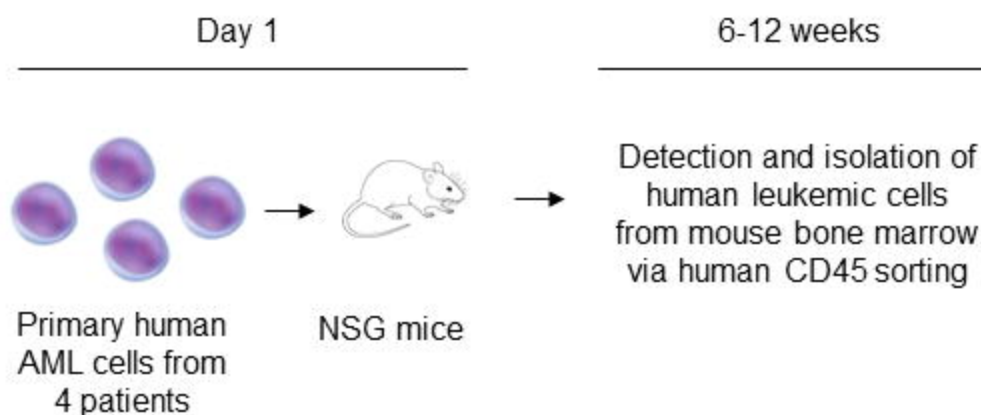
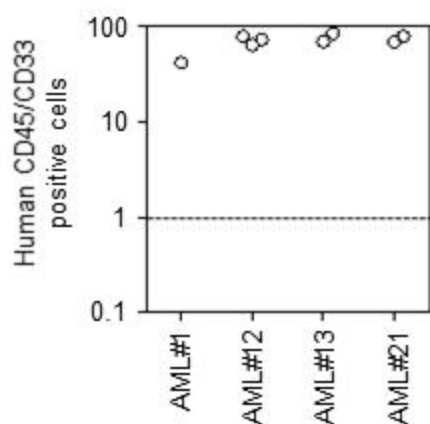


Figure 2

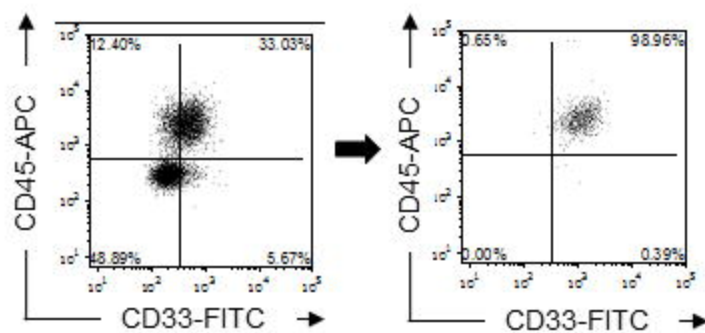
a



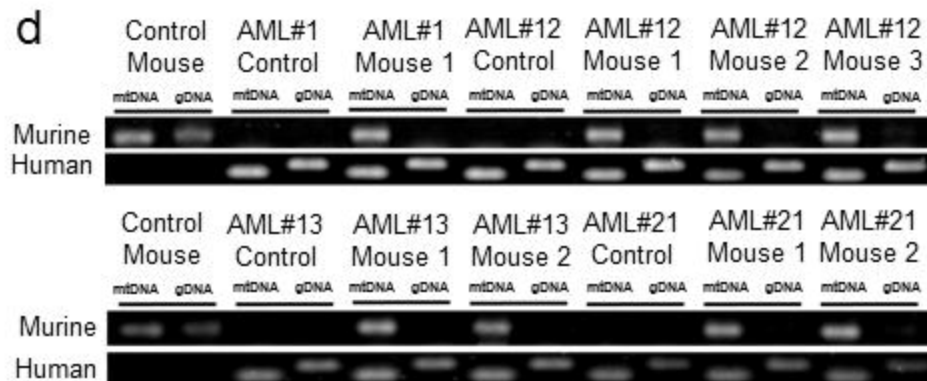
b



c



d



e

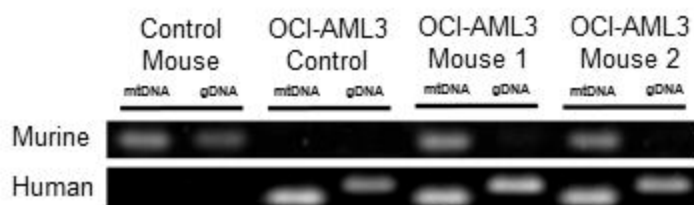


Figure 3

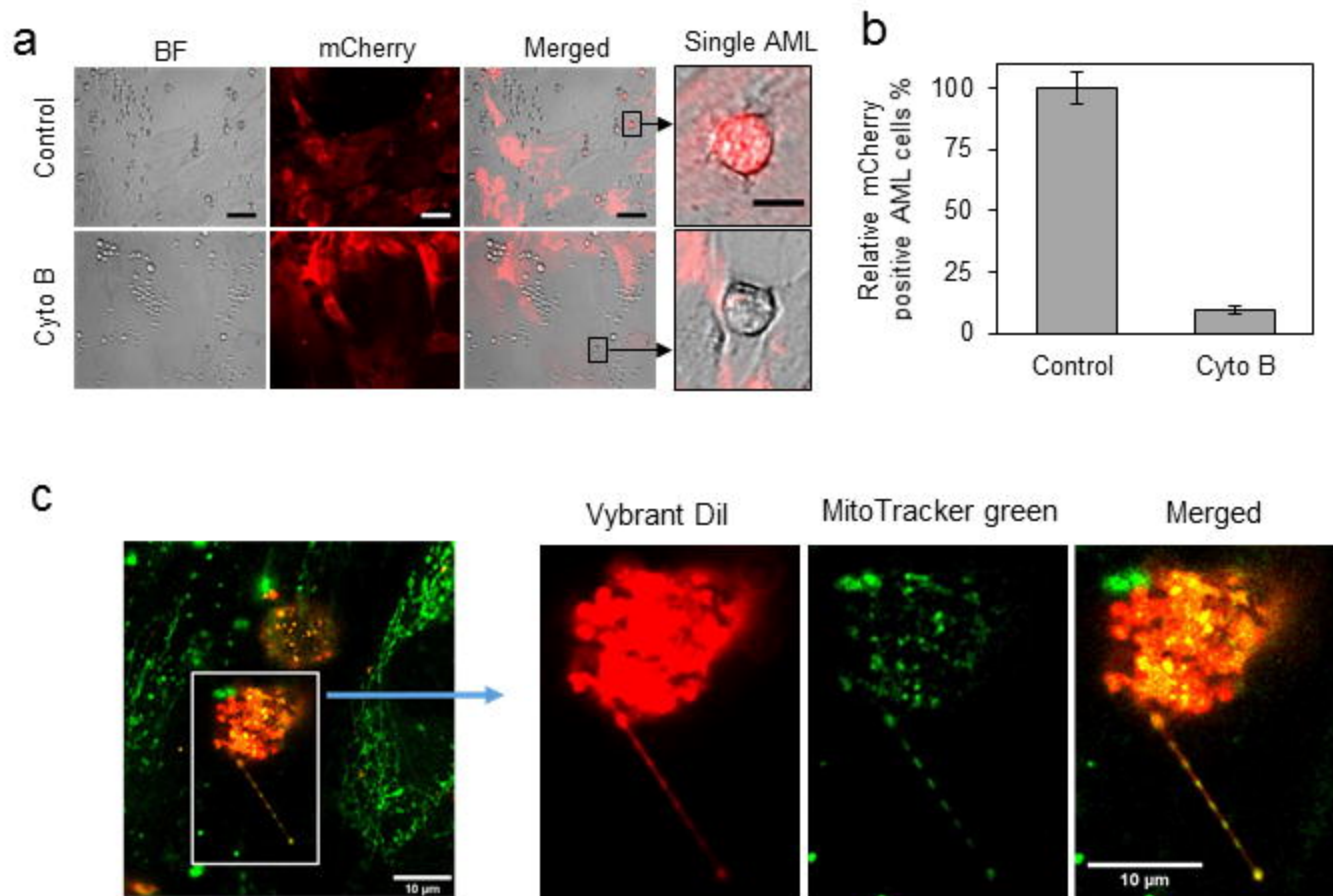


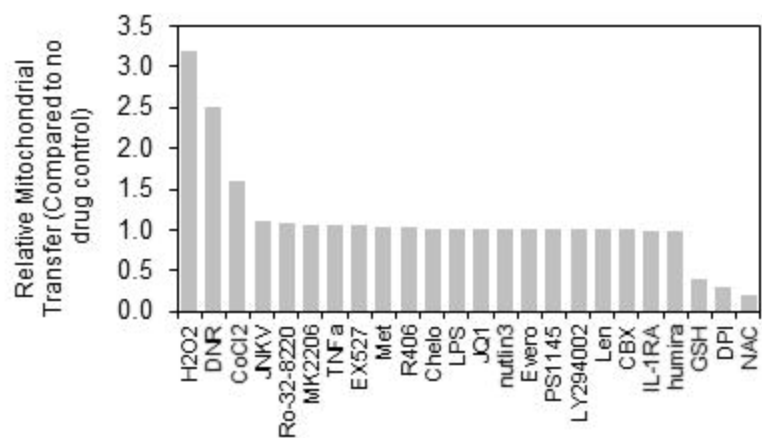
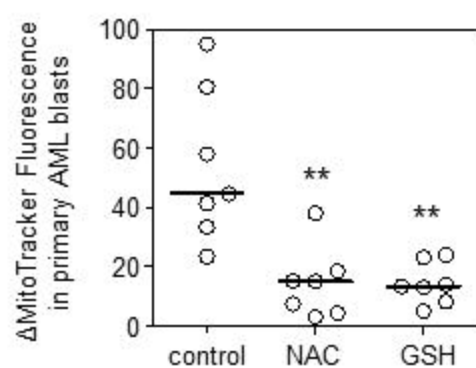
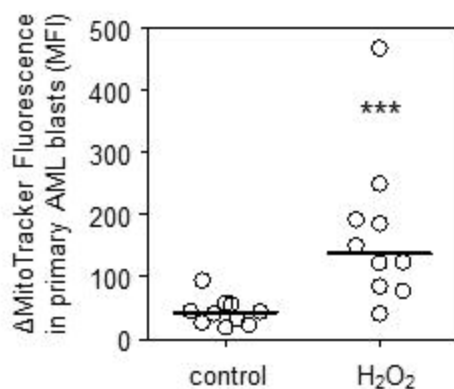
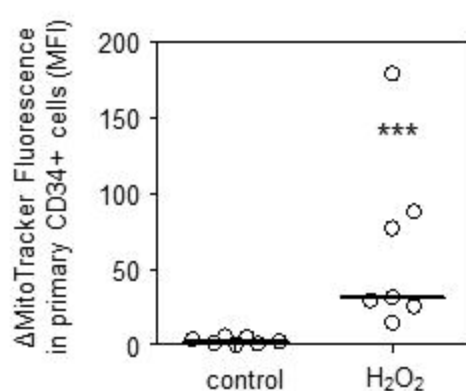
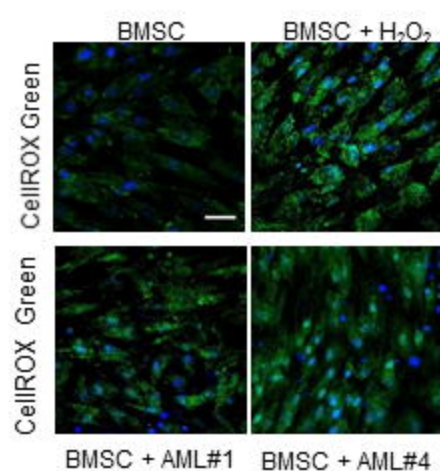
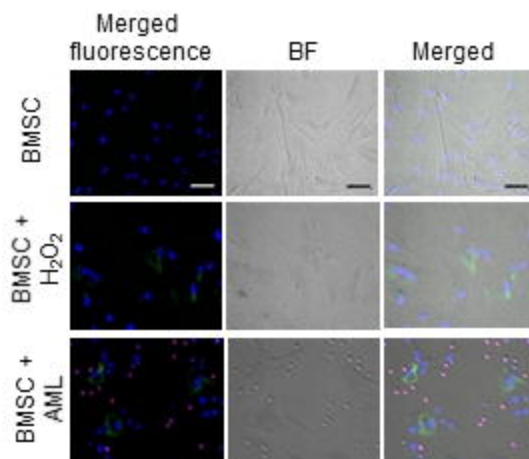
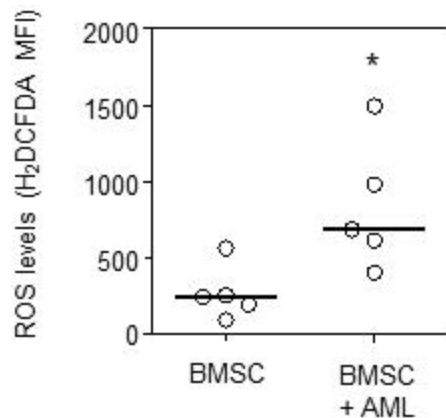
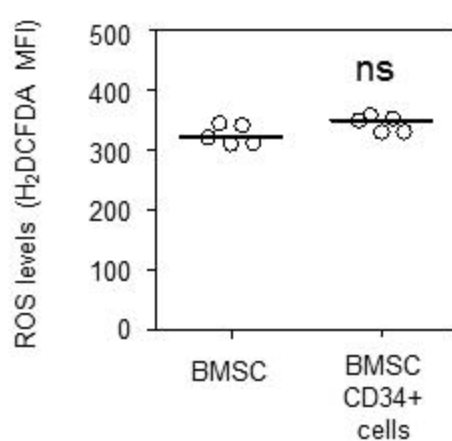
Figure 4**a****b****c****d****e****f****g****h**

Figure 5

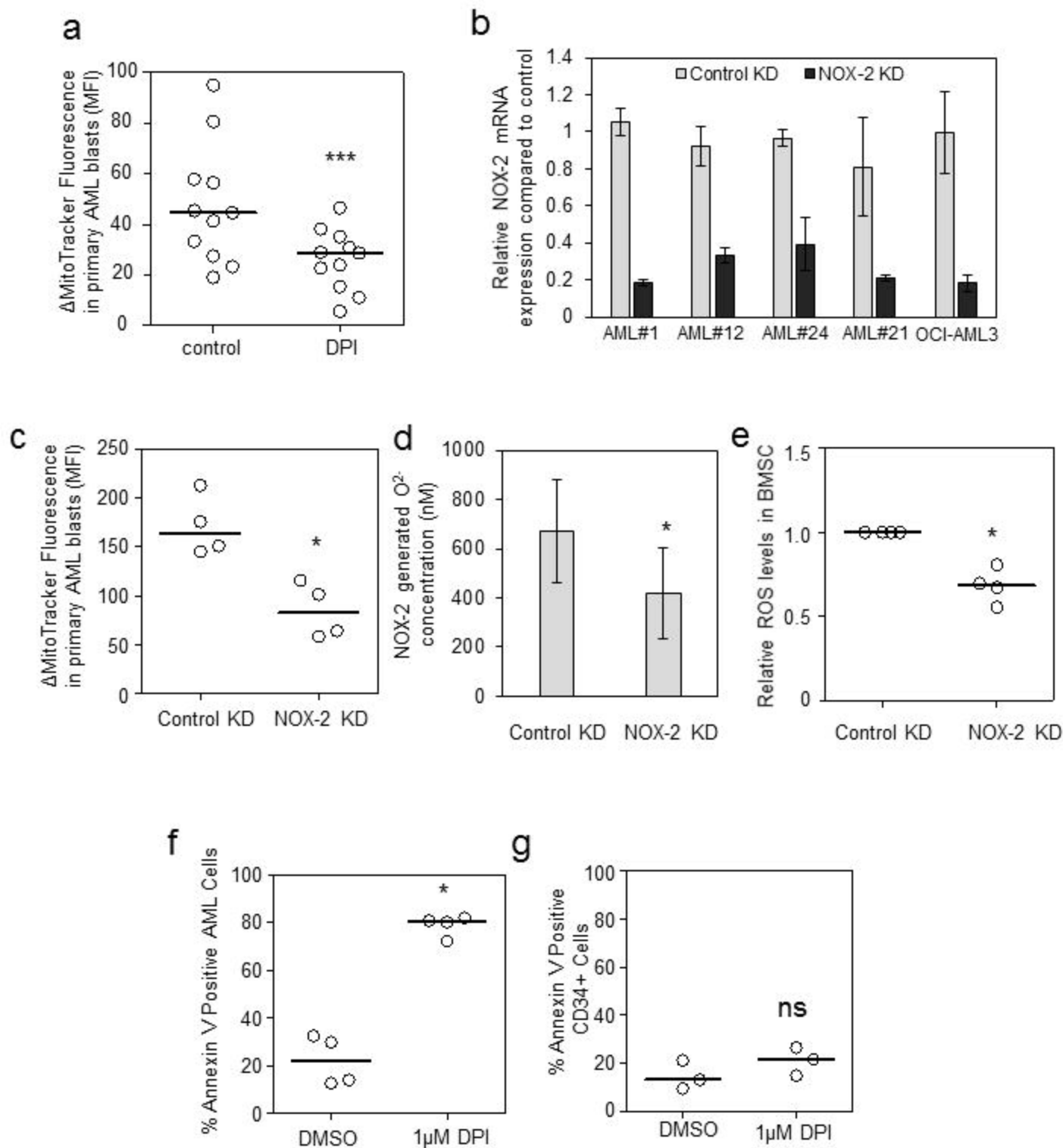


Figure 6

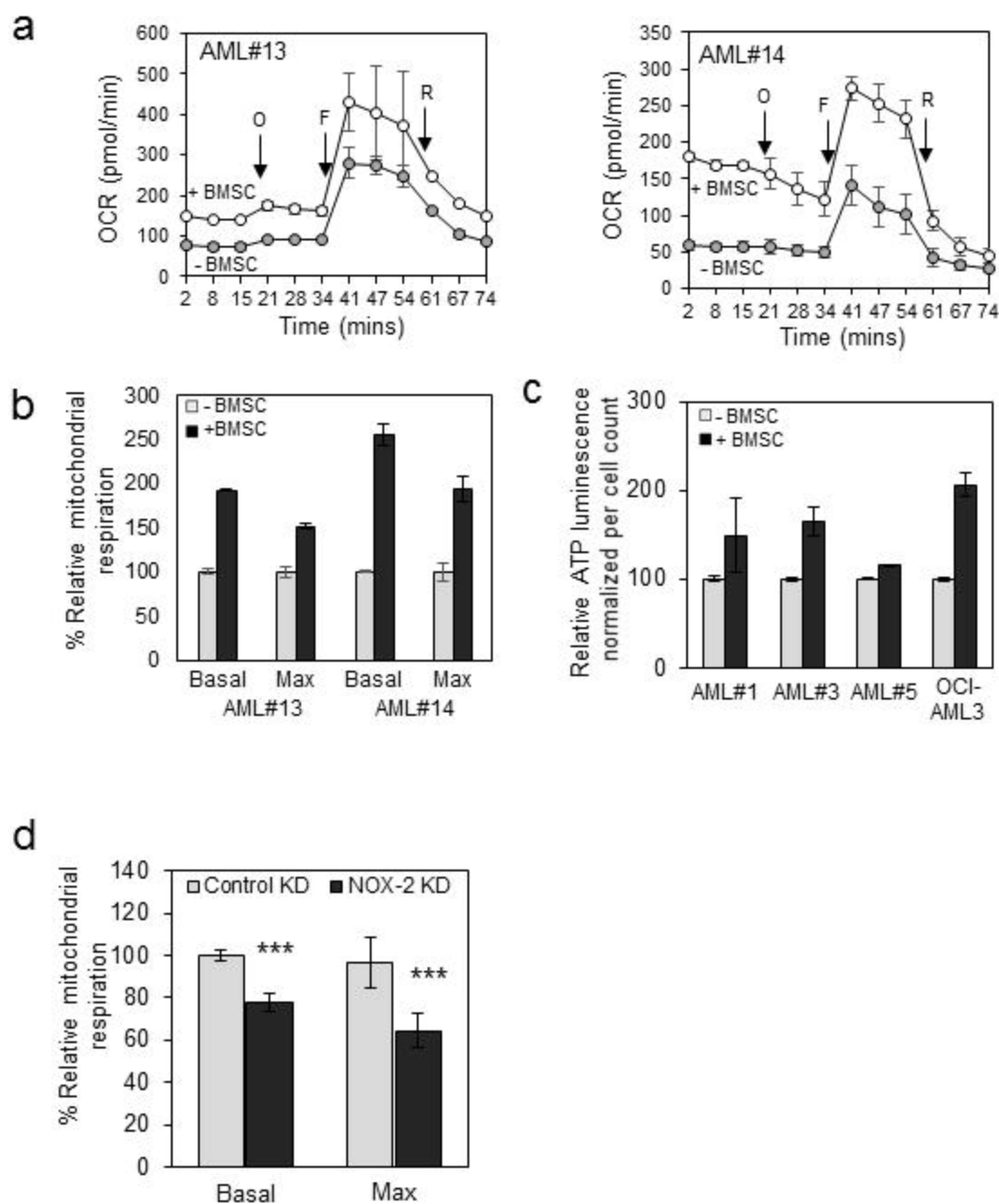


Figure 7

